ADVANCES IN ATMOSPHERIC SCIENCES, VOL. 39, JANUARY 2022, 80–96

• **Original Paper** •

Comparison of the Anthropogenic Emission Inventory for CMIP6 Models with a Country-Level Inventory over China and the Simulations of the Aerosol Properties

Tianyi FAN*[1], Xiaohong LIU[2], Chenglai WU[3], Qiang ZHANG[4], Chuanfeng ZHAO[1], Xin YANG[1], and Yanglian LI[1]

[1]*College of Global Change and Earth System Science*, *Beijing Normal University*, *Beijing* 100875, *China*

[2]*Department of Atmospheric Sciences*, *Texas A&M University*, *College Station*, *Texas* 77843, *USA*

[3]*International Center for Climate and Environment Sciences*, *Institute of Atmospheric Physics*, *Chinese Academy of Sciences*, *Beijing* 100029, *China*

[4]*Department of Earth System Science*, *Tsinghua University*, *Beijing* 100091, *China*

(Received 25 March 2021; revised 6 August 2021; accepted 23 August 2021)

ABSTRACT

Anthropogenic emission inventory for aerosols and reactive gases is crucial to the estimation of aerosol radiative forcing and climate effects. Here, the anthropogenic emission inventory for AerChemMIP, endorsed by CMIP6, is briefly introduced. The CMIP6 inventory is compared with a country-level inventory (i.e., MEIC) over China from 1986 to 2015. Discrepancies are found in the yearly trends of the two inventories, especially after 2006. The yearly trends of the aerosol burdens simulated by CESM2 using the two inventories follow their emission trends and deviate after the mid-2000s, while the simulated aerosol optical depths (AODs) show similar trends. The difference between the simulated AODs is much smaller than the difference between model and observation. Although the simulated AODs agree with the MODIS satellite retrievals for country-wide average, the good agreement is an offset between the underestimation in eastern China and the overestimation in western China. Low-biased precursor gas of SO_2, overly strong convergence of the wind field, overly strong dilution and transport by summer monsoon circulation, too much wet scavenging by precipitation, and overly weak aerosol swelling due to low-biased relative humidity are suggested to be responsible for the underestimated AOD in eastern China. This indicates that the influence of the emission inventory uncertainties on simulated aerosol properties can be overwhelmed by model biases of meteorology and aerosol processes. It is necessary for climate models to perform reasonably well in the dynamical, physical, and chemical processes that would influence aerosol simulations.

Key words: anthropogenic emission inventory, AerChemMIP, CMIP6, MEIC, aerosol, CESM2

Citation: Fan, T. Y., X. H. Liu, C. L. Wu, Q. Zhang, C. F. Zhao, X. Yang, and Y. L. Li, 2022: Comparison of the anthropogenic emission inventory for CMIP6 models with a country-level inventory over China and the simulations of the aerosol properties. *Adv. Atmos. Sci.*, **39**(1), 80–96, https://doi.org/10.1007/s00376-021-1119-6.

Article Highlights:

- Discrepancies exist between the anthropogenic emission inventory for CMIP6 and the country-level emission inventory, MEIC.
- Yearly trends of the simulated aerosol burden deviate between CMIP6 and MEIC after the mid-2000s, but not for the aerosol optical depth.
- Influence of the emission inventory on aerosol simulations is overwhelmed by model dynamical, physical, and chemical processes.

1. Introduction

Anthropogenic emissions of aerosols and precursor gases have dramatically changed the composition of the atmosphere since the beginning of the industrial era. Aerosols, by either scattering solar radiation or acting as cloud condensation or ice nuclei, exert significant influence on the energy budget of the Earth–atmosphere system, imposing an overall cooling effect at the top of atmosphere (Forster et al.,

* Corresponding author: Tianyi FAN
Email: fantianyi@bnu.edu.cn

2007; Shindell et al., 2013; Smith et al., 2020). The knowledge of aerosol burden, optical depth, and other properties is crucial to quantifying the aerosol radiative forcing and climate effects.

Global climate models are important tools used to investigate the impacts of anthropogenic aerosols on radiative forcing and climate change. In the latest Coupled Model Intercomparison Project phase 6 (CMIP6; Eyring et al., 2016), aerosols are specified as one of the near-term climate forcers (NTCFs). The Aerosol Chemistry Model Intercomparison Project (AerChemMIP) endorsed by CMIP6 is designed to quantify the impacts of aerosols and chemically reactive gases (i.e., the NTCFs) on climate and air quality (Collins et al., 2017). To avoid the uncertainty introduced by using diverse aerosol and gas emission datasets, models participating AerChemMIP use consistent historical anthropogenic emissions for aerosols and reactive gases. This practice can be traced back to the Atmospheric Chemistry and Climate Model Intercomparison Project (ACCMIP) of the Coupled Model Intercomparison Project phase 5 (CMIP5) (Lamarque et al., 2013; Shindell et al., 2013). The emission inventory adopted by models participating in AerChemMIP is developed by the Community Emission Data System (CEDS, Hoesly et al., 2018; Feng et al., 2020) and designed with the purpose of being similar to the country-level inventories when available and plausible. The country-level emission inventories are relatively reliable since they take into account the updated information about statistics, technology innovation, and control policies of the country. For China, the CEDS model is calibrated to the Multi-resolution Emission Inventory for China (MEIC; Zhang et al., 2009; Li et al., 2017).

One of the main purposes of the AerChemMIP is to investigate how the uncertainties in historical NTCF emissions affect radiative forcing estimates (Collins et al., 2017). Emission rates are important in simulating the aerosol burden and properties, especially for countries like China where the economy is growing rapidly. The CMIP5 models tend to underestimate the aerosol optical depth (AOD) in East Asia (Shindell et al., 2013). The model low biases are suggested to result from underestimated anthropogenic emissions (Liu et al., 2012b). The low bias over eastern China is reduced by replacing the default CMIP5 emission inventory with the MEIC inventory (Fan et al., 2018). Now that the AerChemMIP/CMIP6 models use a new emission inventory developed by CEDS, it is a good time to evaluate the difference between the default CMIP6 inventory (i.e., the CEDS estimates) and the MEIC inventory, as well as the aerosol properties over China simulated by the global climate models.

In this study, we aim to demonstrate the uncertainty of the CMIP6 emission inventory and the impact of emission on the aerosol simulation. We attempt to realize the goal by comparing the yearly trend, monthly variation, and spatial distribution of CMIP6 and MEIC emission inventories over China, simulating aerosol properties using the Community Earth System Model version 2 (CESM2) with the two inventories, evaluating the model results against observations, and analyzing the cause of model biases. We also would like to know the impact of other processes (e.g., meteorology, chemistry, and aerosol processes) on the simulated aerosol properties. In section 2, we describe the details of CMIP6 and MEIC emission inventories, the model configuration, and the observational datasets used to evaluate the model results. In section 3, we compare the two emission inventories, evaluate the model performance against observations, and analyze the differences of simulated aerosol properties by using the two emission inventories. Conclusions are provided in section 4.

2. Data description and model configuration

2.1. *The CMIP6 emission inventory*

The CMIP6 inventory was developed by CEDS, which is well documented in Hoesly et al. (2018) and Feng et al. (2020). Here, we provide a brief introduction and highlight its relevance with the country-level emission inventories. The CMIP6 inventory is designed to be consistent over time and be similar to country-level inventories when available, complete, and plausible. The dataset is consistent over time because the emissions are estimated under the same activity data, or so-called "underlying drivers", for each particular sector, country, and fuel type. The total anthropogenic emission (E) is calculated by

$$E_{e,c,s,f,t} = A_{c,s,f,t} F_{e,c,s,f,t} \,, \tag{1}$$

where A is the activity (or the "driver"), F is the emission factor, e is the emission species, c is the country, s is the sector, f is the fuel (where applicable), and t is the year. The activity data are usually the fuel consumption for combustion emissions and the population for non-combustion emissions. The emission factor reflects the combined impacts of fuel types, technologies, and abatement/control measures on emissions and is therefore subject to large uncertainties. Firstly, a default global emission dataset (1960/71–2014) was constructed using driver and emission factor data on an annual basis by countries, sectors, species, and fuel types. Secondly, to be similar to the country-level inventories, the default dataset was scaled to authoritative country-level emission inventories when available to match the total emission estimates in these countries on a sector basis. Note that the scaling process modifies the default emissions, but activity estimates remain the same. That is to say, the emission per unit activity (i.e., the emission factor) was modified in the process of scaling. Thirdly, the inventory was also extended to historical trend before year 1970 with activity and emission factors back in time separately. In this way, the activity data actually "drives" the emission trend over time for most species and sectors. Finally, emissions by countries were gridded using normalized spatial proxy data for each country, which were primarily gridded emissions from EDGAR v4.2

(EC-JRC/PBL, 2012) and HYDE population (Goldewijk et al., 2011).

Numerous CEDS working sectors were defined and investigated (Table A1 and Table A2 in Hoesly et al., 2018). The working sectors follow the International Energy Agency (IEA) energy statistics sector definitions for combustion emissions and the EDGAR definitions for non-combustion emissions. To generate gridded emission datasets, the emissions in working sectors are aggregated by country and then into 16 intermediate sectors (Table 6 in Hoesly et al., 2018) for each country. The emissions are spatially distributed into gridded emissions by using normalized spatial proxy distributions for each country. Gridded emissions were further aggregated to nine final sectors: agriculture, energy, industrial, transportation, residential–commercial–other, solvents, waste, international shipping, and aircraft. The CEDS emission inventory does not include sources from open burning, which have anthropogenic contributions (e.g., forest and grassland fires or agricultural open waste burning). The biomass burning emission for CMIP6 is included in van Marle et al. (2017).

For China, CEDS was used to calibrate the emissions to the MEIC dataset developed for the MIX inventory, which is an intermediate version between MEIC v1.0 and v1.2. (Zhang et al., 2009; Li et al., 2017). Five species are scaled including SO_2, NO_x, NH_3, non-methane volatile organic compounds (NMVOCs), and carbon monoxide (CO) for 2008, 2010, and 2012. Black carbon (BC) and organic carbon (OC) emissions were not calibrated but were from the default emissions using the Speciated Pollutant Emission Wizard (SPEW; Bond et al., 2007). This is because BC inventory estimates were only available in a few country-level inventories, and OC estimates were even less available. Thus, CEDS retains the consistent BC and OC estimates from SPEW for all countries.

We noticed that the sector definitions do not exactly match between CEDS and MEIC inventories, which could introduce discrepancies in the emission estimates. The scaling of CEDS to MEIC is based on sectors which are chosen to be broad, as opposed to detailed, because it is often unclear if the sector definitions of CEDS and MEIC are comparable. Additionally, underlying driver data in MEIC and CEDS may not match. Scaling detailed sectors may result in unrealistically scaled emission factors at a detailed sector level. The scaling process operates on emission estimates for which detailed sector information exists in both CEDS and MEIC. In a few cases, when some sectors are known to be missing in MEIC, the default CEDS emission estimates were added after scaling (e.g., waste burning and SO_2 emission from non-ferrous metal smelting). As a result, the CEDS emission total can be larger than MEIC. More details are discussed in section 3.1.1.

2.2. *The MEIC emission inventory and the merging methodology with the CMIP6 inventory*

MEIC is a bottom-up emission inventory framework developed and maintained by Tsinghua University (Streets et al., 2006; Zhang et al., 2007a, b, 2009; Lei et al., 2011). MEIC uses a technology-based approach which keeps track of China's energy statistics and technology renewal and represents changes of emission characteristics from different sectors, fuels, products, combustion/process technologies, and emission control technologies in recent years (Li et al., 2017). The advantage of MEIC is the inclusion of a unit-based power plant emission database (Wang et al., 2012; Liu et al., 2015), a high-resolution vehicle emission modeling approach (Zheng et al., 2014), and an explicit NMVOC speciation assignment methodology (Li et al., 2014). MEIC is widely used in climate, air quality, and environmental studies.

We attempt to construct a global 30-year (1986–2015) monthly emission dataset of SO_2, BC, primary organic matter (POM), NO_x, and NH_3 for CESM2 with MEIC providing the emission rates for China. A "mosaic" strategy is adopted to replace the CMIP6 emissions with MEIC over China while the rest of the world is kept the same as the CMIP6 emissions. The developer's team has been updating the versions of the MEIC dataset, and the long-term dataset used in our study is based on MEIC v1.3. OC mass is multiplied by a factor of 1.4 to represent the total organic mass (i.e., convert to the mass of POM). Since there is large uncertainty in the emission of VOCs that form secondary organic aerosols (SOAs) and the chemistry model in CESM2 uses a different philosophy of organic speciation than the CB05 chemical mechanism in MEIC, we decide not to merge the VOC species. A previous study (Fan et al., 2018) shows that a 46.9% difference in the VOC emission between CMIP5 and MEIC [(MEIC-CMIP5)/CMIP5] leads to a 17.4% difference in the SOA optical depth (~0.005). Using this relationship as an approximation, a multi-year (2000 to 2014) averaged difference of 52.9% in total VOC emission estimates between CMIP6 and MEIC ((MEIC-CMIP6)/CMIP6, 18.15 Tg per year and 27.74 Tg per year in CMIP6 and MEIC, respectively) may lead to a 22.2% difference in the SOA optical depth (~0.006).

Only five CEDS anthropogenic sectors (industry, energy, domestic, transportation, and agricultural) are replaced by MEIC. The five MEIC sectors are aggregated from several sub-sectors following the IPCC sector definitions as described in Table S5 of Li et al. (2017). We referred to the sector mapping in Table S5 in the electronic supplementary materials (ESM) of Li et al. (2017). As mentioned in section 2.1, the MEIC sectors are broadly matched with the CEDS sectors, although differences in sector definition do exist. MEIC does not include emissions from some sources, such as waste burning, SO_2 emission from non-ferrous metal smelting, and open biomass burning.

Since the available aerosol/gas species, grid resolution, and time frequencies are different for various time periods, we adopt a separate merging methodology for each time period (Table 1). For years 2000 to 2015, MEIC is developed to characterize the year-to-year evolution of China's monthly mean emissions for various chemical spe-

Table 1. The merging methodology of anthropogenic emissions* in the MEIC inventory from 1986 to 2015.

	1986–89	1990–99	2000–2015
SO_2 **	CMIP6 scaled to MEIC in 2000	CMIP6 scaled to MEIC in 2000	MEIC
BC	CMIP6 scaled to MIC in 1990	MIC	MEIC
POM	CMIP6 scaled to MIC in 1990	MIC	MEIC
NO	CMIP6 scaled to MEIC in 2000	CMIP6 scaled to MEIC in 2000	MEIC
NH_3	CMIP6 scaled to MEIC in 2000	CMIP6 scaled to MEIC in 2000	MEIC

*The anthropogenic emissions in the MEIC inventory include energy, industrial, residential, and transportation sectors for SO_2, BC, POM, and NO_x, and an additional agricultural sector for NH_3. **5% of the SO_2 mass is emitted as primary sulfate aerosol.

cies. The horizontal resolution of MEIC is 0.2° by 0.2°, which enables MEIC to provide more details of energy and industrial emissions and to show more concentrated residential and transportation emissions over populated eastern China than the CMIP6 emissions at a resolution of 0.5° by 0.5°. We merge the five species that are related to the emission or formation of aerosols (SO_2, BC, POM, NO_x, and NH_3). For years 1990 to 1999, we use the gridded emissions for BC and POM from the Modeling Inventory and Constrains (MIC) project on anthropogenic emissions, which is developed by the same team as MEIC at Tsinghua University. The country-wide total emission rates for BC and POM are available on a year-to-year basis, while the spatial distribution is updated every five years. There are no monthly data for these years, and we apply the CMIP6 monthly data to produce the MEIC monthly variation. For other species (e.g., SO_2, NO_x, and NH_3) that are not provided by MIC, we scale the CMIP6 data to match the MEIC emission rates in the year 2000 by using the following equation:

$$E_{\mathrm{MEIC},m,y} = E_{\mathrm{CMIP6},m,y}\frac{E_{\mathrm{MEIC},2000}}{E_{\mathrm{CMIP6},2000}}, \quad (2)$$

where $E_{\mathrm{MEIC},m,y}$ and $E_{\mathrm{CMIP6},m,y}$ are monthly averages of MEIC and CMIP6 emissions for years 1990 to 1999, respectively, m represents month, y represents year, and $E_{\mathrm{MEIC},2000}$ and $E_{\mathrm{CMIP6},2000}$ are the annual averages of MEIC and CMIP6 emissions for the year 2000, respectively. For 1986–1990, MEIC data is unavailable. We scale the annual CMIP6 emissions of SO_2, BC, POM, NO_x, and NH_3 from 1986 to 1989 to obtain the MEIC emission rates by using the following equation:

$$E_{\mathrm{MEIC},m,y} = E_{\mathrm{CMIP6},m,y}\frac{E_{\mathrm{MEIC},1990}}{E_{\mathrm{CMIP6},1990}}, \quad (3)$$

where $E_{\mathrm{MEIC},m,y}$ and $E_{\mathrm{CMIP6},m,y}$ are the monthly averages of MEIC and CMIP6 emissions for years 1986 to 1989, respectively, and $E_{\mathrm{MEIC},1990}$ and $E_{\mathrm{CMIP6},1990}$ are the annual averages of MEIC and CMIP6 emissions for year 1990, respectively.

The number emission fluxes are calculated from the mass fluxes. The mass to number conversion is based on $E_{\mathrm{number}} = E_{\mathrm{mass}}/\left(\frac{\pi}{6}\rho D_{\mathrm{v}}^{3}\right)$, where D_{v} is the volume-mean emitted diameter and ρ is the aerosol particle density (Liu et al., 2012b).

When input to CESM2, both MEIC and CMIP6 emission datasets are regridded to the model resolutions of 0.9° by 1.25° using areal conservative interpolation, which means that the country-wide total anthropogenic emissions should be conserved after regridding if we calculate it by adding up emission rates (in units of mass per area per time) and multiplying by the area of the grids. However, in practice, the regridding procedure does not exactly conserve the total anthropogenic emissions because the area defined as China has changed due to the change of resolution, in this case from a fine resolution (i.e., MEIC at 0.25° by 0.25° or MIC at 0.5° by 0.5°) to a coarse one (i.e., model resolution of 0.9° latitude by 1.25° longitude). The effect of the regridding on our analysis should be minor because the difference due to regridding is under 3% for various species. It should also be noted that regridding based on area of the grid boxes is not equivalent to regridding according to the spatial proxies. When producing the gridded data, different spatial proxies are used for different emission sources. For MEIC, locations of emitting facilities were used to derive gridded emission for large sources, while spatial proxies, such as population density, road networks, and land use information, are used to allocate emissions of areal sources (Li et al., 2017). In spite of this, the result of areal conservative regridding is acceptable if we go from a fine resolution to a coarse one since the emitting sources are likely to be included within the larger grids under the coarser resolution.

2.3. *CESM2 model configuration*

CESM2 is the latest generation of the coupled climate/Earth system model developed by the community from the National Center for Atmospheric Research (NCAR), universities, and other research institutions, with Community Atmospheric Model version 6 (CAM6) as the atmospheric component (Danabasoglu et al., 2020). We initialize the model in 1979 from the restart files of a long, fully coupled atmosphere–ocean–sea ice historical run (the "HIST" run). We then run the Atmospheric Model Intercomparison Project (AMIP)-type (i.e., atmospheric and land components–only) simulation with prescribed sea surface temperatures and sea ice concentrations for 37 years, with the first 7 years (1979–85) as spin-up and the last 30 years (1986–2015) for analysis. The horizontal resolution is 0.9° by 1.25° (latitude

by longitude), with 32 vertical levels up to the model top of 2.26 hPa. This is referred to as the "low-top" configuration, with a relatively coarse stratospheric configuration and no prognostic chemistry module for ozone and other stratospheric constituents. There are 151 gas-phase chemistry, 65 photolysis, and 287 kinetic reactions in the troposphere, with improved representation of ozone and secondary organic aerosol precursors (Emmons et al., 2020). The aerosols are treated by the four-mode version of the Modal Aerosol Model (MAM4, Liu et al., 2016; Lu et al., 2021). The four modes are an Aitken mode (containing sulfate, SOA, and sea salt), an accumulation mode (containing sulfate, BC, POM, SOA, sea salt, and dust), a coarse mode (containing sulfate, sea salt, and dust), and a primary carbon mode (containing BC and POM). The primary carbon mode is to explicitly treat the microphysical aging of primary carbonaceous aerosols. Nitrate aerosol was incorporated with gas-phase nitrogen chemistry and included in AOD calculation in this study. The Cloud Layer Unified By Binormals (CLUBB; Golaz et al., 2002; Larson, 2017) moist turbulence scheme handles the treatment of the shallow-convection, boundary layer, and grid-scale condensation. The updated Morrison-Gettelman cloud microphysics scheme (MG2; Gettelman and Morrison, 2015) prognoses both mass and number concentration of four classes of hydrometers (cloud drop, cloud ice, rain, and snow).

2.4. *Observations for evaluating the model results*

To evaluate the model performance, we compared the model results with satellite observations and reanalysis data. The Moderate Resolution Imaging Spectroradiometer (MODIS) on board the Earth Observing System (EOS) Aqua and Terra satellites has been widely used for aerosol observations (Remer et al., 2008). The collection 6.1 Level 3 1° by 1° monthly mean AOD (550 nm) product from the Aqua satellite (MYD08, Levy et al., 2013; Sayer et al., 2014) is used in this study. The merged dark target (DT) and deep blue (DB) dataset is adopted considering its advantage in gap-filling by combining the best of DT and DB datasets. The MODIS Aqua L3 monthly dataset is sampled at the satellite overpass time of ~1330 LST and excludes the unsuccessful retrievals due to dense cloud, ice/snow surface, etc. In contrast, our model output provides monthly averages, which could cause the comparison to suffer from a temporal sampling issue (Schutgens et al., 2016; Park et al., 2018). Considerable temporal sampling errors are found for yearly and monthly averages, and the sign and magnitude of the errors are model- and region-dependent. Over eastern China, models tend to overestimate AOD without temporally collocated sampling, while over deserts, models generally tend to underestimate AOD if a collocated comparison is not considered. Unfortunately, we were not able to analyze the temporal sampling error in this study because hourly (or 3-hourly) model output frequency is needed, but we only output monthly data due to the large storage resource required for two 37-year runs. We will carry out the analysis based on monthly data but keep in mind the potential biases of monthly averages due to temporal sampling when comparing with MODIS.

Atmospheric oxidation is important for the conversion of gas-phase precursors (e.g., SO_2) to aerosol acids (e.g., sulfuric acid). We used the total column O_3 product retrieved by the Ozone Monitoring Instruments (OMI) on board the EOS Aura satellite (Bhartia, 2002; Ziemke et al., 2011) to evaluate the model. Total Ozone Mapping Spectrometer (TOMS)-like daily Level 3 1° × 1° gridded data (OMTO3d) in the year 2015 are time-averaged and spatially regridded to compare with modeled column O_3.

SO_2 is the precursor gas of sulfate aerosol. Properly simulated SO_2 concentration is a premise of correct sulfate aerosol modeling. We evaluate the simulated SO_2 concentration by the SO_2 column mass density from the Modern-Era Retrospective Analysis for Research and Applications version 2 (MERRA-2, Randles et al., 2017).

Meteorological conditions affect the gas-phase chemical reaction rates, aerosol transport, and removal processes. The horizontal wind, relative humidity, and temperature simulated by the model are validated with the ERA5 reanalysis (Hersbach et al., 2019). For precipitation, we compared the model results with the Global Precipitation Climatology Project (GPCP) monthly analysis version 2.3 (Adler et al., 2018).

3. Results

3.1. *Comparisons of the CMIP6 and MEIC datasets*

3.1.1. *Yearly trend*

The emissions of aerosols and their precursor gases have experienced dramatic changes in China from 1986 to 2015 due to rapid economic growth, increased consumption of fossil fuel, innovated technology, and more stringent control measures. The CMIP6 and the MEIC inventories consistently show that emission rates of precursor gases and primary aerosols gradually rise since 1986, level off in the mid-1990s, increase dramatically after 2000, and stabilize around the mid-2000s (Figs. 1a–e). However, the yearly trends become different between the two inventories, especially after the mid-2000s. Table 2 provides the averages and linear trends of emissions for each 10-year period (1986–95, 1996–2005, and 2006–15) and for the 30-year period as a whole (1986–2015). The emission of SO_2, as the precursor gas of sulfate aerosol, decreased dramatically after 2006 in the MEIC inventory [–45.12 Tg (30 yr)$^{-1}$, significant, evaluated at 5% significant level hereinafter], while the change in the CMIP6 inventory was comparatively small [–2.74 Tg (30 yr)$^{-1}$, insignificant]. The emission rates of BC and POM in MEIC level off after 2006 and drop after 2013, while they keep growing steadily after 2006 as estimated by the CMIP6 inventory and level off at a higher rate than the MEIC maximums after 2013 (Figs. 1b and 1c). The emissions of nitrogen oxides (NO_x, represented as NO), which lead to the formation of nitrate aerosols, in both emis-

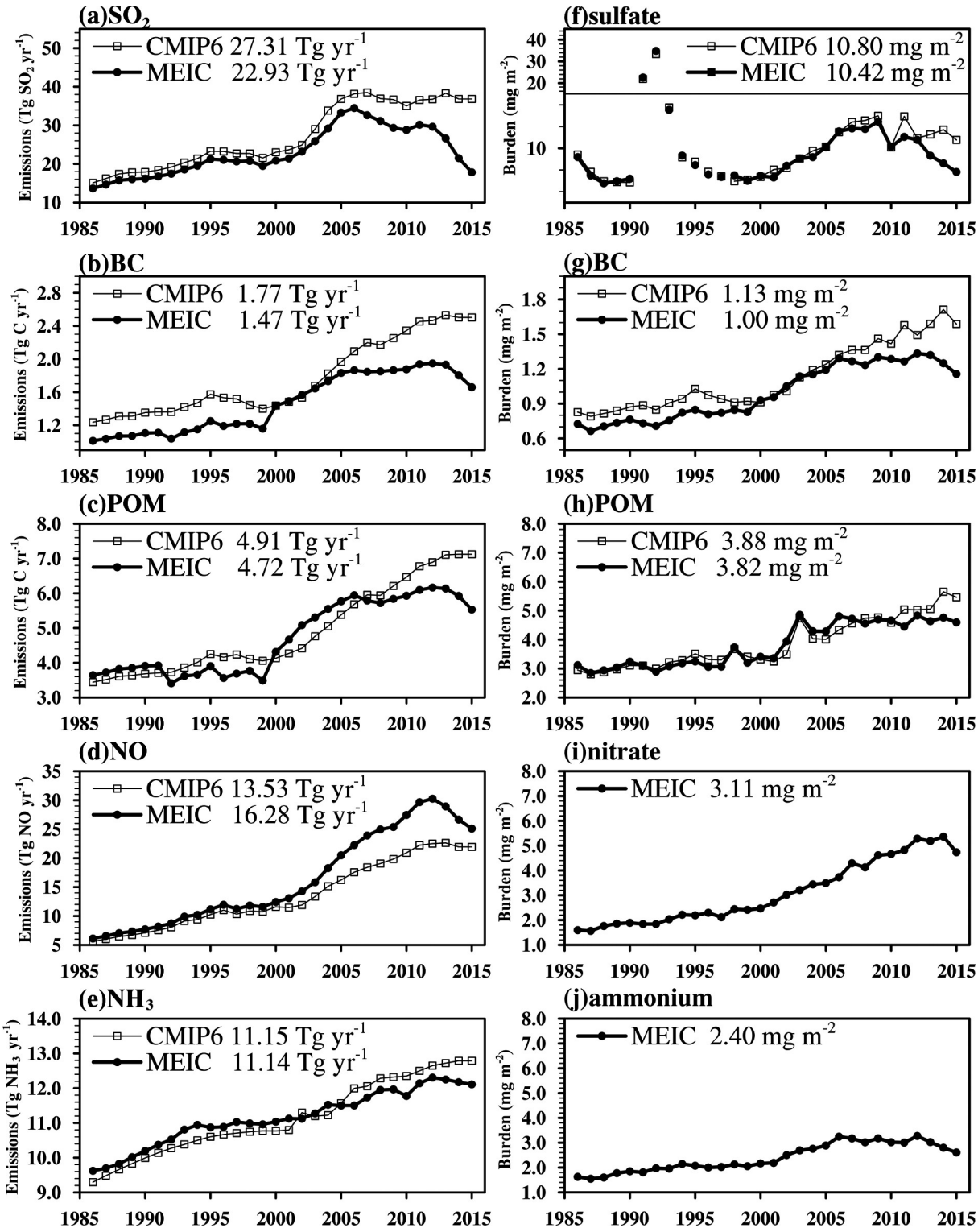

Fig. 1. Trends of the emission rates for SO_2, BC, POM, NO, and NH_3 over China from 1986 to 2015. The numbers in the legend are averages over the 30 years. The horizontal line in Fig. 1f corresponds to 15 mg m^{-2}, below and above which the *Y*-axis labels are both in increments of 2 mg m^{-2}.

sion inventories experience periods of gradual growth from 1986 to the mid-2000s, rapid growth from the mid-2000s to 2012, and decline since 2012. The decrease after 2012 is more evident for MEIC than CMIP6 (Fig. 1d). The emissions of ammonia (NH_3), which is the precursor gas for ammonium aerosols, grow persistently from 1986 to 2015 in both inventories, except that the MEIC inventory shows a slight decrease after 2012 (Fig. 1e). The discrepancies mentioned above are due to the fact that the MEIC emission inventory keeps track of the renewal of energy structure and

Table 2. Averages and trends* of AOD, aerosol emissions, and burdens for different time periods. AOD averages are unitless and AOD trends are in the unit of (30 yr)$^{-1}$. Emission averages are in units of Tg yr^{-1} and emission trends are in units of Tg (30 yr)$^{-1}$. Burden averages are in units of mg m^{-2}, and burden trends are in units of mg m^{-2} (30 yr)$^{-1}$.

	1986–95		1996–2005		2006–15		1986–2015	
Emission inventory	CMIP6	MEIC	CMIP6	MEIC	CMIP6	MEIC	CMIP6	MEIC
AOD	0.27	0.28	0.28	0.28	0.34	0.34	0.29	0.30
	(0.12)	(0.15)	(**0.12**)	(**0.19**)	(0.02)	(−0.01)	(**0.10**)	(**0.09**)
AOD dust	0.16	0.16	0.16	0.15	0.15	0.15	0.16	0.15
	(−0.03)	(−0.02)	(−0.04)	(−0.04)	(−0.04)	(−0.01)	(−0.01)	(**−0.02**)
AOD MODIS	–	–	–	–	0.34	–	–	–
	–	–	–	–	(−0.13)	–	–	–
SO_2 emission	18.71	16.99	26.15	23.58	37.06	28.22	27.31	22.93
	(**23.49**)	(**22.05**)	(**44.04**)	(**37.71**)	(−2.74)	(**−45.12**)	(**26.87**)	(**15.52**)
sulfate burden	7.98	7.91	8.18	8.10	11.7	10.53	9.44	8.95
	(2.71)	(3.28)	(**9.38**)	(**8.58**)	(−3.82)	(**−13.18**)	(**5.35**)	(**3.45**)
BC emission	1.37	1.10	1.58	1.45	2.35	1.86	1.77	1.47
	(**0.92**)	(**0.56**)	(**1.40**)	(**2.31**)	(**1.51**)	(−0.26)	(**1.45**)	(**1.11**)
BC burden	0.88	0.75	1.02	0.97	1.49	1.27	1.13	1.00
	(**0.61**)	(**0.42**)	(**1.02**)	(**1.43**)	(**1.14**)	(−0.14)	(**0.92**)	(**0.76**)
POM emission	3.74	3.75	4.46	4.52	6.53	5.91	4.91	4.72
	(**2.24**)	(−0.07)	(**3.84**)	(**8.32**)	(**5.34**)	(0.08)	(**4.13**)	(**3.19**)
POM burden	3.08	3.07	3.65	3.72	4.92	4.67	3.88	3.82
	(**0.61**)	(**0.42**)	(**1.02**)	(**1.43**)	(**1.14**)	(−0.14)	(**0.92**)	(**0.76**)
NO emission	7.63	8.30	12.26	14.10	20.70	26.45	13.53	16.28
	(**15.15**)	(**16.37**)	(**17.51**)	(**28.18**)	(**16.56**)	(14.87)	(**19.25**)	(**26.42**)
nitrate burden	–	1.88	–	2.76	–	4.68	–	3.11
	–	(**2.05**)	–	(**4.70**)	–	(**4.34**)	–	(**4.15**)
NH_3 emission	10.02	10.29	10.98	11.15	12.45	11.99	11.15	11.14
	(**4.35**)	(**4.83**)	(**2.83**)	(**1.98**)	(**2.84**)	(**2.07**)	(**3.61**)	(**2.60**)
ammonium burden	–	1.84	–	2.34	–	3.03	–	2.40
	–	(**1.95**)	–	(**3.16**)	–	(**−1.45**)	–	(**1.73**)

*Trends in bold font are statistically significant at 5% significance level. – MODIS AOD products are not available during 1985–95 or only available for a few years during 1996–2005. Nitrate and ammonium concentration in the CMIP6 emission run were not output.

emission abatement measures in recent years in response to the urgent need of improving the air quality in China. One of the control policies that has had a profound impact on recent air quality in China is the "Atmospheric Ten Articles" proposed by the State Council in 2013.

We notice that the emission estimates in CEDS do not exactly match those in MEIC in the scaling years of 2008, 2010, and 2012. One factor that could lead to the difference is the evolution of MEIC dataset versions. The CEDS model that produces the CMIP6 dataset is scaled to an intermediate version between MEIC v1.0 and v1.2, while the version used in our study is based on MEIC v1.3. Another factor could be the sector definition of CEDS. CEDS add sectors that MEIC does not provide (e.g., waste burning and SO_2 emission from non-ferrous metal smelting). For power plants that function to generate power and produce heat, CEDS attributes both sectors to the power sector. MEIC attributes the power generation to the power sector and the heat production to the industry sector. This mainly affects the proportion of SO_2 and NO in power and industry sectors. According to CEDS, heat production is responsible for about 10.0% and 15.3% of the total SO_2 and NO emissions from energy production, respectively. Another example is metal smelting. CEDS includes emissions due to the production of both Iron-Steel and non-ferrous metals, while MEIC only includes emissions from the production of Iron-Steel. Industrial combustions of non-ferrous metals contribute about 2%–3% of SO_2, BC, POM, and NO industrial emissions.

Comparisons of the yearly trends by sector for each species are provided for selected years in Fig. S17. Here, we compared five sectors (industry, power, residential, transportation, and agricultural). A reduction of SO_2 emission from the power sector since 2006 due to the application of new desulfurization technology is evident in MEIC; the reduction is not as obvious in CMIP6 as it is in MEIC. The deviation of SO_2 emission between the two inventories after 2012 is mainly due to the industry and the power sectors. There is a major difference in power sector emissions for BC, POM, and NMOVC in the CMIP6 and MEIC inventories. The BC, POM, and NMVOC emissions from power sectors in MEIC are greatly reduced compared to CMIP6, which is due to the consideration of clean fuel use in MEIC. MEIC reports higher emission in the industry sector for BC, POM, NO, and NMVOC. The NO and NMVOC emissions in the transportation sector of MEIC are also higher than CMPI6. The higher emissions of NO and NMVOC in the MEIC industry and transportation sectors result in a higher total anthropogenic emission in MEIC than CMIP6.

In summary, the differences between the CMIP6 and MEIC inventories exist over China in the scaling years of 2008, 2010, and 2012 because (1) MEIC dataset version evolves after serving as country-level inventory for CEDS

scaling, and (2) sector definitions sometimes mismatch. On top of that, the long-term yearly-trend difference exists because (1) only three years (2008, 2010, and 2012) of MEIC data were used in the scaling so that the trends can deviate due to the different treatment of the emission factors (e.g., new technology, more stringent control policy) and the driver (e.g., fuel consumption, population), (2) BC and OC emissions were not calibrated by MEIC but from the SPEW data, and (3) only the emission totals of China were used for scaling so that the spatial distributions were different.

3.1.2. *The spatial distribution*

The spatial distributions of the CMIP6 and MEIC emissions are quite consistent with each other (Fig. 2). Anthropogenic emissions of all species show an "eastern-high and western-low" pattern. Here, we refer to the "Heihe-Tengchong Line" as the divide of eastern and western China (see Fig. S1 for the geographical locations). We further divide eastern China into northern and southern China, whose emission distributions are generally distinct from each other, according to the "Qinling-Huaihe Line" along about 33°N. Emission hot spots are located in populated and economically developed regions, for example, the Northeastern China Plain (NECP), Northern China Plain (NCP), Yangtze River Delta (YRD), Sichuan Basin (SCB), and Pearl River Delta (PRD). The CMIP6 SO_2, BC, and POM emissions are higher compared to MEIC emissions over most parts of China, except over Guizhou and Shanxi Provinces. The CMIP6 datasets show lower NO and NH_3 emissions in eastern China and higher emissions in western China than the MEIC datasets.

3.1.3. *Monthly variation*

The CMIP6 and MEIC emission inventories are very similar in terms of the country-wide averaged monthly variation (Fig. 3). The SO_2, BC, and POM emissions of the two inventories peak in the winter. The MEIC NO emission shows more complex monthly variation than the CMIP6 NO emission. The NH_3 emissions in both inventories have first peaks in May and second peaks in September. It should be noted that the monthly variation can be location- and time-dependent. We use the most frequent months of maximum emission (MFMME) to demonstrate the idea. The MFMME at each location (i.e., a grid in the dataset) is defined as the most frequent month during 2000 to 2015 in which the maximum monthly emission in the year occurs. Likewise, we can define the second MFMME, which is the second most frequent month of maximum monthly emission of the year, during the 16 years. We do not include the period from 1986 to 1999 because MEIC does not provide monthly variations in this time period. MFMMEs for SO_2, BC, and POM in the CMIP6 inventory are January for almost everywhere in China (see Fig. S2 in the supplementary materials), which means the monthly variations of these species are relatively location-independent. The NO emissions peak in January over eastern China and July over western China most frequently. The NH_3 emissions peak in May over eastern China and May or July over western China most frequently. Thus, the monthly variations of NO and NH_3 are location-dependent. The relative frequency of occurrences (RFOs) of MFMMEs are equal or close to 100% in the CMIP6 inventory for all species, and there barely exist second MFMMEs. This means that emissions all peak in the same month during the 16 years, and the monthly variations are, so-to-speak, time-independent. The MFMMEs in the MEIC inventory are both location- and time-dependent (Fig. S3). The SO_2, BC, and POM emissions peak in winter most frequently everywhere, and the NO emission peaks in winter most frequently for eastern China and in summer for western China, consistent with the CMIP6 emission. However, second MFMMEs appear, and their RFOs cannot be ignored. The RFOs of MFMMEs and second MFMMEs add up to less than 100% (91.6% to 94.5%) for SO_2, BC, POM, and NO, which means the monthly variations of MEIC have more diversities in time and space.

3.2. *Evaluation of the model performance over China*

3.2.1. *Yearly trend*

Global models have difficulties in simulating the aerosol properties in regions where historical anthropogenic emissions are not well documented, and they tend to underestimate AOD over China (Shindell et al., 2013; Liu et al., 2012b; Fan et al., 2018). We first evaluate the simulated AOD by CESM2 against observations in this section, and then we analyze the differences of simulated aerosol properties due to the emission inventories in section 3.3.

The CESM2 simulated AODs averaged over China are comparable with the MODIS retrieved AOD (Fig. 4a, 0.34 for CESM2/CMIP6 run, 0.33 for CESM2/MEIC run, and 0.37 for MODIS from 2006 to 2015). Linear regression analysis gives a decreasing trend of –0.13 $(30\ yr)^{-1}$ for MODIS retrievals from 2006 to 2015 and a small change for the model simulations [0.02 $(30\ yr)^{-1}$ for CESM2/CMIP6 run and –0.01 $(30\ yr)^{-1}$ for CESM2/MEIC run], but neither the observed nor the simulated AOD trend is statistically significant (Table 2). Although the yearly trend looks reasonable for the country-wide averages, regional trends show large discrepancies between model and observations. The modeled regional averaged AODs using the CMIP6 inventory are underestimated by a factor of 1.6 and 1.2 for northern and southern China, respectively, and overestimated by a factor of 1.2 for western China from 2006 to 2015 (Figs. 4b–d). These biases over eastern China and dust-aerosol dominated western China cannot be explained by the temporal sampling issue between model and MODIS observation. Model results using the CMIP6 inventory show increasing trends for both northern and southern China [0.05 $(30\ yr)^{-1}$ and 0.19 $(30\ yr)^{-1}$, respectively, both significant], while MODIS retrieval shows an increasing trend [0.07 $(30\ yr)^{-1}$, not significant] for northern China but a decreasing trend for southern China [–0.23 $(30\ yr)^{-1}$, significant].

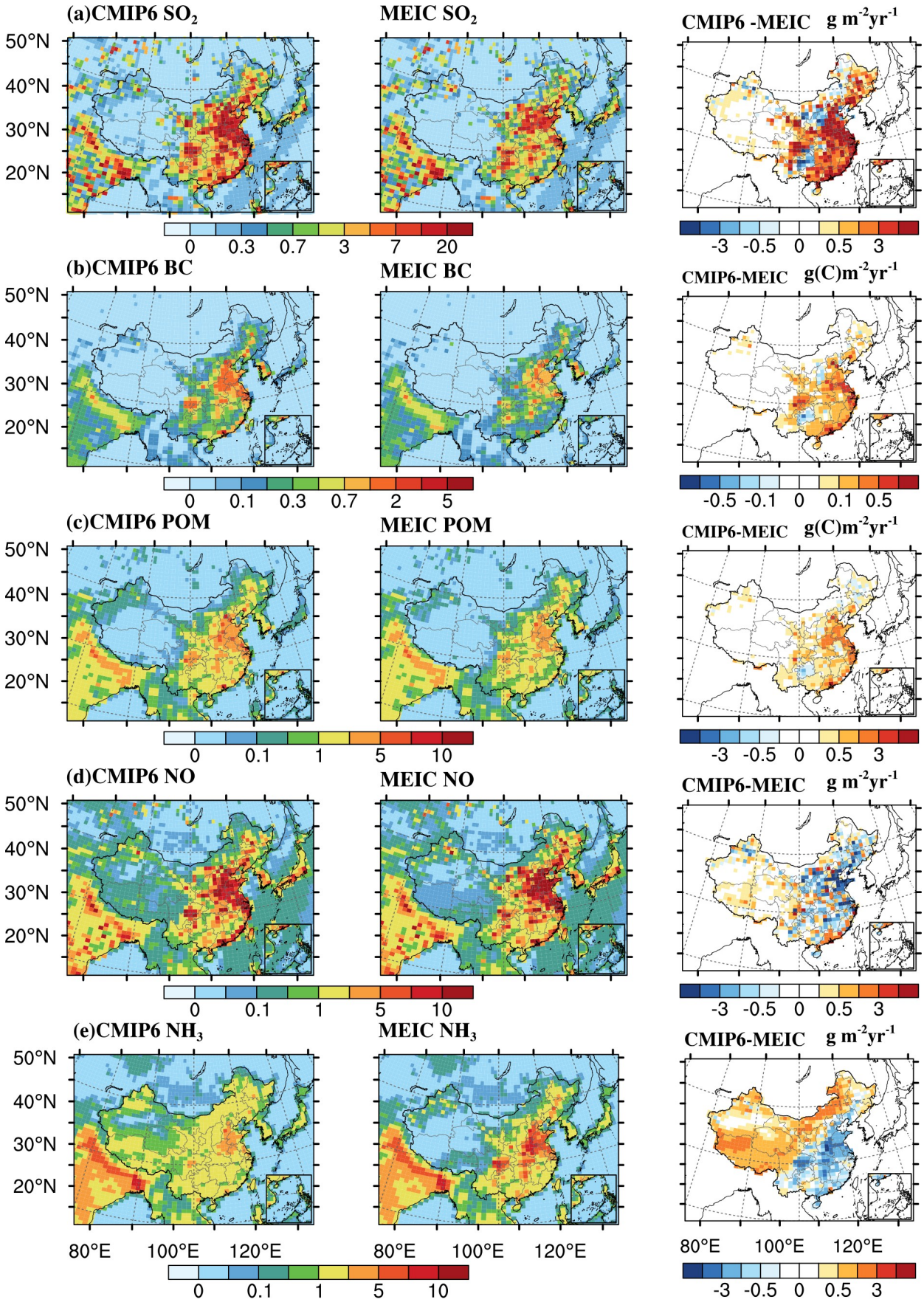

Fig. 2. Spatial distribution of CMIP6 and MEIC (a) SO_2, (b) BC, (c) POM, (d) NO, and (e) NH_3 emissions in 2015.

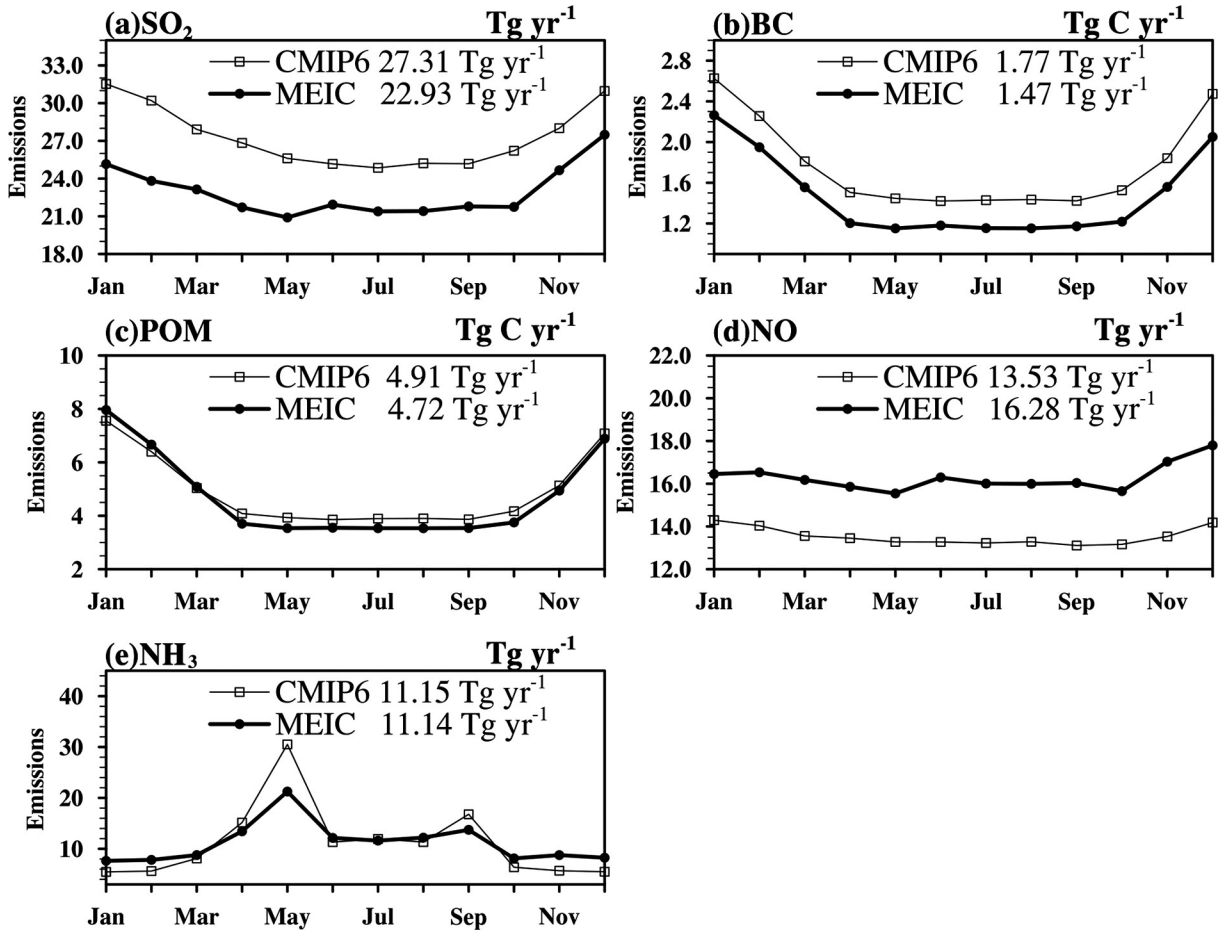

Fig. 3. Monthly variations of the emission rates for (a) SO_2, (b) BC, (c) POM, (d) NO, and (e) NH_3 over China averaged from 1986 to 2015.

3.2.2. *Monthly variation*

Figure 5 shows the monthly variation of AOD over China and its three regions. The simulated monthly variation of AOD over China has a strong correlation with the monthly variation of dust AOD and agrees with the MODIS retrievals (Fig. 5a). This is mainly due to the dominant role of dust aerosol in the AOD variations over western China, where the model performs well compared to the MODIS retrievals, although it underestimates in spring and winter and overestimates in summer and autumn (Fig. 5d). Wu et al. (2020) compared the dust modeled by CESM2 with satellite observations and found that the monthly variation of dust optical depth in their results also showed a major peak in April and a minor peak in September, as in ours. The minor peak exists in the CALIOP retrievals but is not seen in MODIS and MISR.

AODs over northern and southern China are less influenced by the dust aerosol, and the monthly variations do not agree with the MODIS retrievals (Figs. 5b and 5c). AOD is underestimated over northern China all year long, there is a lack of variation compared with MODIS, and the model fails to predict the maximums in February, May, and June. AOD over southern China is overestimated in the winter and underestimated in other seasons, and the model is unable to simulate the maximums in March, April, and June as in the MODIS retrievals. The observed maximums in northern and southern China comply with the efficient gas-phase oxidation rate of SO_2 by OH radical to form H_2SO_4 at high temperature as well as higher concentration of OH radical due to efficient photochemical reaction rates in summer (Li and Han, 2012; Zhang et al., 2013; Fan et al., 2018). Moreover, high relative humidity in the summer favors hygroscopic growth of aerosol particles, which leads to higher AOD (Liu et al., 2012a).

3.2.3. *Spatial distribution*

There are large biases in the spatial distribution of AOD between the simulations and observation (Fig. 6). Taking the year 2015 for example, the AODs over NECP and NCP were underestimated by CESM2, and they were overestimated over SCB and Taklamakan Desert (TD) (Fig. 6d). In many cases the bias is out of the range of the MODIS retrieval uncertainty ($\pm 0.05 \pm 0.15\tau$). The differences between simulations using the two emission inventories are much smaller compared to the differences between simulations and observations (Fig. 6c). The underestimation of AOD over NECP is most evident in winter (Fig. 4Sl). The underestimation in NCP can be found all year long (Figs.

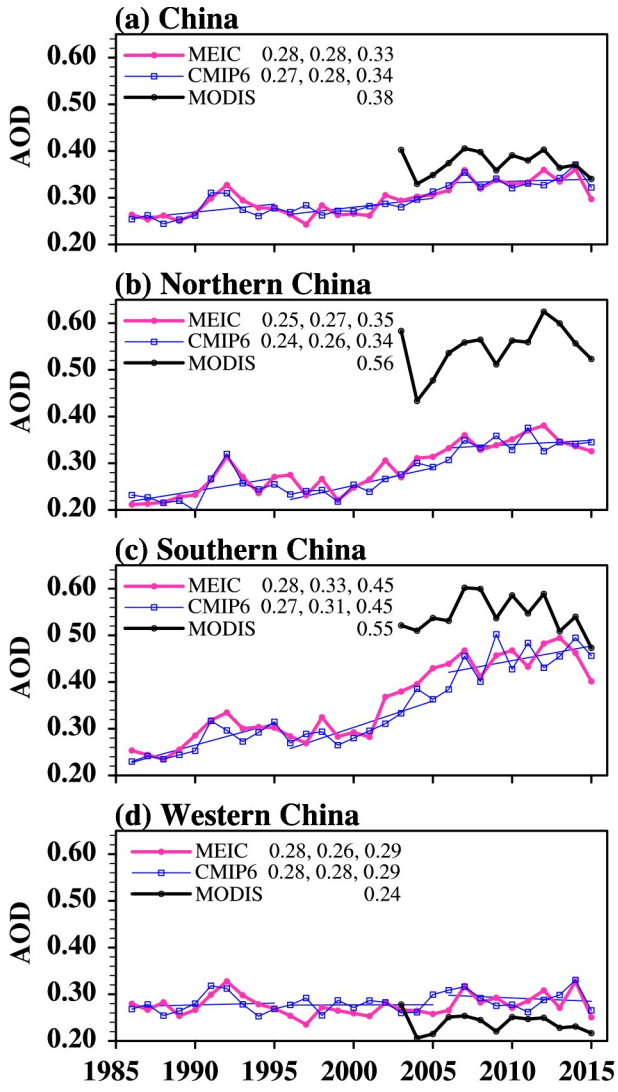

Fig. 4. Yearly trends of AOD in visible wavelength over (a) China, (b) northern China, (c) southern China, and (d) western China from 1986 to 2015. The three columns of numbers in the legend are AOD averages over 1986–95, 1996–2005, and 2006–15, respectively. Region definitions can be found in Fig. S1.

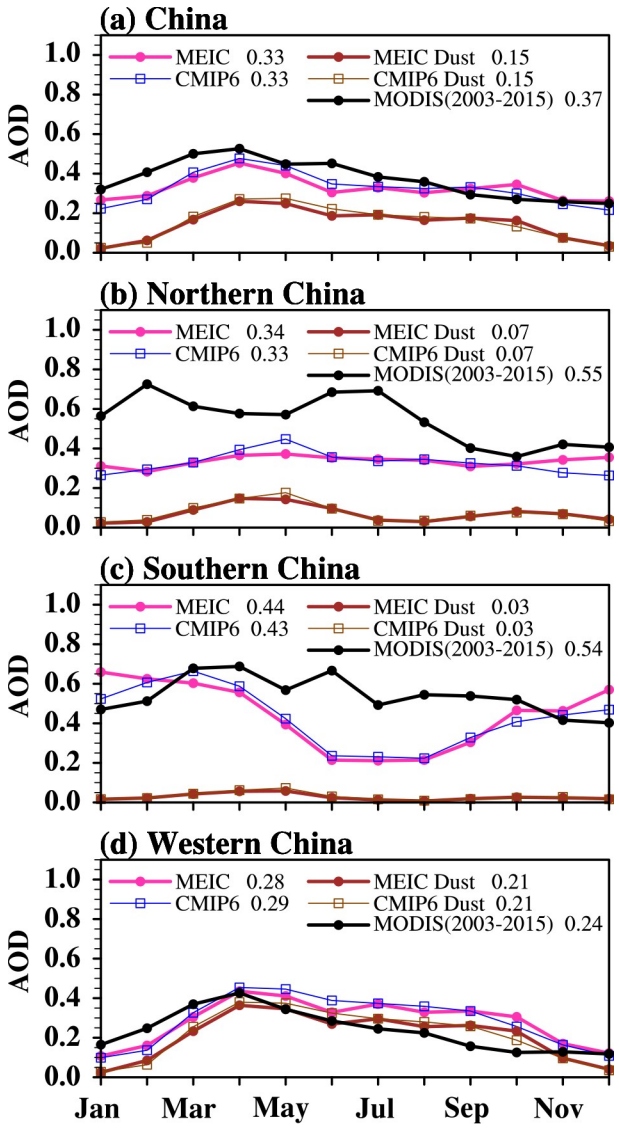

Fig. 5. Monthly variations of AOD and dust AOD in the visible wavelength simulated by CESM2 with CMIP6 and MEIC emissions, compared with the MODIS retrieved AOD in the visible wavelength for (a) China, (b) northern China, (c) southern China, and (d) western China. Values in the legends are averaged from 2003 to 2015.

4Si–l). The overestimation over SCB occurs in spring, autumn, and winter and is largest in winter. The model biases are persistent over the entire period (Fig. S5 for summer and Fig. S6 for winter).

What explains the AOD biases in the model? To answer this question, we examine the emissions for various species and the meteorological conditions that are related to aerosol formation, transport, swelling, and removal. The spatial distributions of emissions (Fig. S7) show little seasonal variation compared to the modeled AOD (Figs. S3b and S3d). Neither evident winter-time enhancement of emissions over SCB nor decrease of emissions over NECP and NCP are observed for any species for both CMIP6 and MEIC inventories, which implies that emissions alone cannot explain the AOD bias in winter (Fig. S4l).

Sulfate aerosol is a major contributor to AOD, and it is formed in the gas phase by oxidation of SO_2 into H_2SO_4 gas and subsequently by nucleation and condensation processes. Therefore, biases in emission will first be reflected in the SO_2 concentration. The column integrated mass of SO_2 is low-biased over NCP as compared with the MERRA-2 SO_2 (Fig. S8), indicating possible underprediction of sulfate aerosol gas-phase formation due to the shortage of precursor. However, the shortage of SO_2 is not likely due to emission alone because the uncertainty range of SO_2 emission is usually small (e.g., only ±12% for MEIC, Zhang et al., 2009) and cannot explain the underestimation by a factor of two for the SO_2 burden. Moreover, the underestimation of SO_2 burden cannot explain the AOD high bias over SCB in winter.

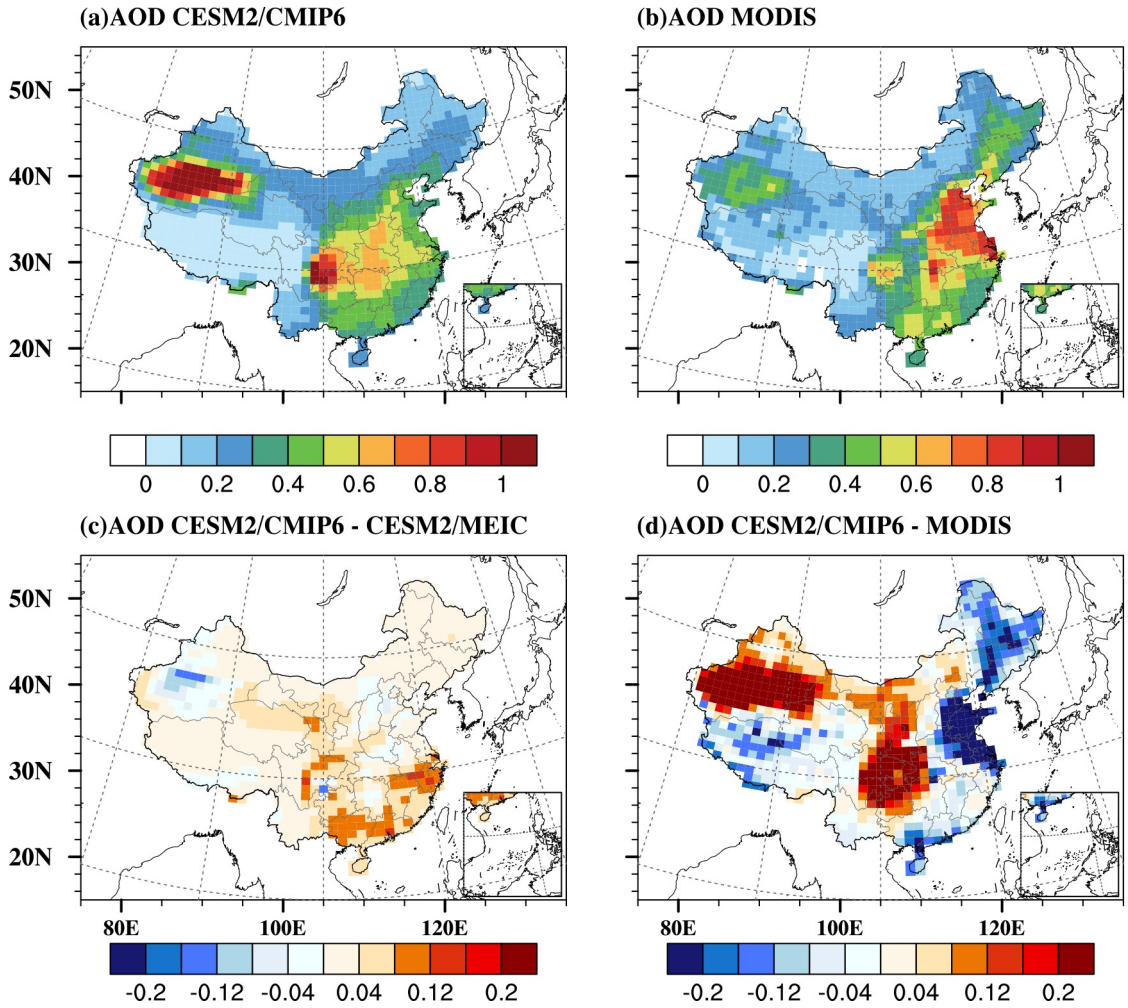

Fig. 6. Spatial distributions of AODs over China in 2015 (a) simulated by CESM2 with CMIP6 emissions and (b) retrieved by MODIS, and the spatial distributions of the difference (c) between simulated AOD by CESM2 with CMIP6 MEIC emission inventories and (d) between simulated AOD with CMIP6 emissions and retrieved AOD by MODIS.

Sulfate is not the only aerosol species that accumulates over SCB during wintertime in the model (Fig. S11), indicating the misleading effects of meteorological conditions in the model that affect all aerosol species. The simulated wind field at 850 hPa shows a false convergence of air flow over SCB in winter as compared with ERA5 reanalysis (Fig. S9), which leads to the artificial accumulation of aerosols. The AOD underestimation over NECP and NCP could be related to the overly strong southerly wind that brings clean marine air mass into eastern China, especially in summer, thus diluting the aerosol-laden air mass and transporting too much aerosol out of NCP and NECP.

The underestimation over NECP and NCP may also be explained by too much aerosol wet scavenging by overestimated precipitation in the model as compared with GPCP precipitation, especially in the summer (Fig. S10). However, the wet scavenging cannot explain the AOD low-bias during summertime in southern China and the high bias during wintertime in SCB.

AOD increases under higher relative humidity (RH) due to hygroscopic growth of aerosol particles. The vertical profiles of RH are compared with the ERA5 reanalysis over three regions where AODs are biased the most (Fig. S12). The AOD low bias around NCP (Region 1) in summer can only be explained by low-biased RH north of 37°E, and the bias in winter corresponds well with low-biased RH below 850 hPa. RH near SCB (Region 2) is mostly underestimated in winter, which cannot explain the AOD high biases there. Around NECP (Region 3) in winter, RH is slightly overestimated from the surface to 300 hPa, which cannot lead to the AOD low bias there.

Temperature affects AOD because SO_2 oxidation to form sulfate aerosol is more efficient at higher temperatures. The modeled temperature is higher than the ERA5 reanalysis over most of eastern China in both summer and winter (Fig. S13), which cannot explain the underestimated AOD over NECP and NCP but may contribute to the wintertime high bias over southern China.

The simulated AOD over TD is overestimated in all seasons (Fig. S4). The CESM2 result is consistent with

MODIS in that the largest AOD happens in the spring. Dust emission is mainly driven by surface wind speed, which is overestimated by CESM2 in both seasons (Fig. S9) and explains the overestimated AOD over the dust source region.

3.3. *Comparison of the simulated aerosol properties using CMIP6 and MEIC emissions*

In this section, we examine the differences of CESM2 simulated aerosol properties introduced by using the CMIP6 and the MEIC emission inventories.

3.3.1. *Yearly trend*

The CESM2 simulated aerosol burdens of various species using both emission inventories generally follow the yearly trend of their anthropogenic and natural sources over the 30-year period of 1986 to 2015 (Figs. 1f–j). All aerosol species generally increase from 1986 until the mid-2000s, but sulfate burden increased abruptly after the eruption of Mt. Pinatubo in 1991 and gradually recovered afterwards. The aerosol burdens in the CMIP6 and MEIC runs began to deviate from each other in the 2000s, just like their emission counterparts. The sulfate burden in the MEIC run decreased much more rapidly after 2006 [–13.18 mg m^{-2} $(30\ yr)^{-1}$, significant, see Table 2] than in the CMIP6 run [–3.82 mg m^{-2} $(30\ yr)^{-1}$, not significant], which results from the much larger decreasing trend of SO_2 emissions in MEIC [–45.12 Tg $(30\ yr)^{-1}$, significant] than in CMIP6 [–2.74 Tg $(30\ yr)^{-1}$, not significant]. The BC and POM burdens show small [both –0.14 mg m^{-2} $(30\ yr)^{-1}$] and statistically insignificant trends from 2006 to 2015 in the MEIC run, while they show positive and significant trends in the CMIP6 run [both 1.14 mg m^{-2} $(30\ yr)^{-1}$]. The BC and POM emissions show exactly the same trends as their burdens, i.e., insignificantly small trends for MEIC and significant positive trends for CMIP6.

In contrast, the yearly averaged AODs simulated in the two runs over China and the three regions are not significantly different, as examined by Student's *t*-test, except for AODs over western China from 1996 to 2005 (Table 2 and Fig. 4). The yearly trends of AODs over China for the two runs are similar (Fig. 4a), with averages of 0.29 and 0.30 and statistically significant increasing trends of 0.10 and 0.09 $(30\ yr)^{-1}$ during 1986–2005 for CMIP6 and MEIC runs, respectively (Table 2). The increasing trends over northern China [0.15 $(30\ yr)^{-1}$, significant, CMIP6 run] and southern China [0.27 $(30\ yr)^{-1}$, significant, CMIP6 run] are larger than the trend over China from 1986 to 2015 [0.10 $(30\ yr)^{-1}$, significant, CMIP6 run]. The differences of the trends between the two runs are mainly over southern China from 2006 to 2015, with 0.19 $(30\ yr)^{-1}$ for the CMIP6 run compared to 0.02 $(30\ yr)^{-1}$ for the MEIC run, while the MODIS retrieval shows a negative trend [–0.23 $(30\ yr)^{-1}$, insignificant)]. The MEIC run agrees better with the MODIS retrieval because the MEIC inventory characterizes the reduction of emissions as a result of innovated technology and control measures (i.e., the installation of flue-gas desulfurization devices since the 2000s, the issue of "Atmospheric Ten Articles" to improve air quality in 2013, etc.).

If we consider the replacement of the CMIP6 inventory with the MEIC inventory as a "perturbation" to the model input, we can quantify the response of the aerosol burden to the emission perturbation. The aerosol burden change and the emission perturbation are calculated by the difference of the burden or emission rates between CMIP6 and MEIC (CMIP6 minus MEIC) divided by the MEIC burden or emission rates. We find that the secondary aerosols (sulfate, nitrate, and ammonium) respond to the emission perturbation in a different way from the primary aerosols (BC and POM). The sulfate burden in the MEIC run is lower than the CMIP6 run by 0.9%, 1.0%, and 11.1% in response to the lower MEIC SO_2 emissions by 10.1%, 10.2%, and 31.3% during 1986–95, 1996–2005, and 2006–15, respectively (Table 2). The changes of the sulfate burden between the two runs are quite small compared to the emission perturbations, and still so after 2006 when the MEIC emission began to deviate considerably from the CMIP6 emission (Figs. 1a, f). In contrast, the differences of BC and POM burdens respond quite consistently to their emission perturbations. The change of BC burden is 17.3%, 5.15%, and 17.3% in response to the BC emissions perturbations of 24.5%, 9.0%, and 25.8% during 1986–95, 1996–2005, and 2006–15, respectively. The change of POM burden is 0.3%, –1.9%, and 5.35% in response to the POM emissions perturbations of –0.3%, –1.3%, and 10.5% during 1986–95, 1996–2005, and 2006–15, respectively. This result confirms the remarks in our previous study that burdens of primary aerosol are closely related to their emissions, and secondary aerosols depend more on the aerosol processes, such as gas-phase formation (Fan et al., 2018).

It is noteworthy that the dust aerosol burden is quite different between the two runs (Fig. S14). Dust is a major contributor to the aerosol burden and AOD, especially in western China and during the spring season. Since the dust emission strongly depends on surface wind speed, we examine the wind speed over the dust source regions. The wind speeds in the dust source regions are overestimated (mainly in winter, see Fig. S9) and show larger annual variation in both runs compared with the ERA5 reanalysis dataset (Fig. S14c). The comparison indicates no preference for one run over the other. A significant difference of surface wind speeds exists between the two runs. Apparently, the difference is due to the change in the anthropogenic emission. Yang et al. (2017) suggested that dust aerosol can modulate wintertime land–sea surface air temperature and influence aerosol burden in eastern China by changing wind patterns. Conversely, the change in anthropogenic aerosols can also induce changes in atmospheric dynamics and further alter the winds that influence the dust emission. We also notice that the differences of dust burden do not necessarily correspond to the differences of surface wind speed between the two runs, which in turn do not necessarily correspond to the difference of anthropogenic emissions (see Fig. 1). This sug-

gests complex interplay between aerosol processes and atmospheric dynamics which should be investigated further in the future.

3.3.2. *Spatial distribution*

Consistent with the emission pattern of SO_2, BC, and POM (Fig. 2, Fig. S7) in 2015, the CMIP6 run shows larger aerosol burden (Fig. S11) and AOD (Fig. 6c) in most parts of China than the MEIC run. The CMIP6 NO and NH_3 emissions are smaller than the MEIC emissions in most parts of eastern China, but the larger simulated sulfate, BC, and POM burdens dominate and result in a larger AOD in the CMIP6 run over eastern China. The dust AOD in the CMIP6 run is smaller than that in the MEIC run over the TD.

To examine the sensitivity of aerosol burdens to the emission perturbations, we calculated the correlation between the monthly aerosol burden change and emission perturbation between the CMIP6 and MEIC runs over the 30 years (Fig. S15). Significant positive correlation can be seen over China for perturbed SO_2, BC, and POM emissions, indicating the evident impact of emission on aerosol burdens. Low correlations often occur in the rims of mountain areas, such as the Loess Plateau, the Inner-Mongolian Plateau, and the Yunnan-Guizhou Plateau, where large altitude gradients are located. This could be due to the strong control of the vertical air circulation on the aerosol burdens. It is interesting that western China, including the Tibetan Plateau and the TD, also shows high correlation, although the anthropogenic emissions are low there. The correlation of dust burden with dust aerosol emission perturbation shows a different pattern than with the anthropogenic emissions. Generally, the correlation is insignificant in western and northeastern China, except for the region east to TD, and it is positive in eastern China, including NCP and southern China. The insignificant correlation in northwestern and northeastern China may result from the dominant role of wind in the transport of dust, which offsets the effect of emission on dust burden.

3.3.3. *Monthly variation*

The monthly AOD variations of the two runs are highly consistent with each other (Fig. 5). Similar monthly variations of emissions are also found between the two inventories in all three regions (Fig. S16). We noticed that the simulated AOD by using the CMIP6 emission in winter (November, December, and January) is lower than that simulated by using the MEIC emission over both northern and southern China, while it is usually higher than or comparable to the AOD simulated by using MEIC in other seasons (Figs. 5b and 5c). The reason for this could be that although the SO_2 and BC emissions in CMIP6 are consistently larger than those in MEIC all year round, the NO_x emissions in CMIP6 for all the seasons and the POM and NH_3 emissions in winter are lower than those in MEIC (Figs. S16a and S16b). Moreover, the conversion rate of SO_2 to H_2SO_4 gas by photolysis-produced oxidants is reduced in winter. Thus, the influences of NO_x, NH_3, and POM emissions on AOD may outweigh the influences of SO_2 and BC emissions in the winter, which makes the wintertime AOD simulated by using the CMIP6 emission lower than that simulated by using the MEIC emission.

4. Conclusions

The question of how anthropogenic emissions affect aerosol radiative forcing draws much attention of the climate research and modeling community. This is one of the key questions to be answered by AerChemMIP, endorsed by CMIP6. The CMIP6 emission inventory, although scaled to country-level inventories (MEIC in the case of China), is different from the country-level inventories due to the scaling procedure, the choice of species to be or not to be scaled, and considerations of technology renewal and control policies. In this study, we aim to answer two questions: 1) What are the differences between the CMIP6 and the MEIC inventories over China? 2) What are the resulting differences of the simulated aerosol properties?

Discrepancies exist between the yearly trends of the two inventories, especially after the mid-2000s. SO_2 emission in MEIC shows a more rapid decrease than the CMIP6 inventory after 2006. BC and POM emissions in MEIC level off around the mid-2000s, while they keep growing in the CMIP6 inventory. NO emission in MEIC is higher and grows more rapidly than the CMIP6 inventory since the year 2000. Spatial distributions of emission rates are similar between the two inventories, but differences also exist. The SO_2, BC, and POM emissions in MEIC are lower than those in the CMIP6 inventory and NO and NH_3 emissions in MEIC are higher than those in the CMIP6 inventory in eastern China. The monthly variations of the country-wide averaged emissions in the two inventories are very similar, with winter maximums and summer minimums for SO_2, BC, and POM,weak monthly variations for NO, and peaks around May and September for NH_3. We also noticed that the monthly variation of the CMIP6 emissions is location-dependent and time-independent, while the MEIC emissions are both location- and time-dependent.

The CESM2 simulated country-wide AOD averages and yearly trends agree well with the MODIS retrieval, but regional differences exist. The model underestimates the regionally averaged AOD by factors of 1.6 and 1.2 over northern and southern China, respectively, and overestimates the AOD by a factor of 1.2 over western China. MODIS shows a decreasing trend over southern China, while the model results show increasing trends with both inventories. The model underestimates the AOD over the Northeastern China Plain and the Northern China Plain in all seasons, overestimates the AOD over Sichuan Basin in the winter, and overestimates the AOD over Taklimakan Desert in all seasons. These biases may result from underestimation of the emissions as well as the model's inability to capture the meteorological variables, most importantly wind and precipitation. By

comparison with satellite observations and reanalysis data, low-biased precursor gas of SO_2, overly strong convergence of the wind field, overly strong dilution and transport by summer monsoon circulation, too much wet scavenging by precipitation, and overly weak aerosol swelling due to low-biased relative humidity are identified to be related to the AOD bias over China.

The differences in simulated aerosol properties between the two runs using the CMIP6 and the MEIC inventories are much smaller than the discrepancies between the simulations and the observations in terms of yearly trend, spatial distribution, and monthly variation. The aerosol burdens simulated by CESM2 show yearly trends similar to their emission trends. The differences of aerosol burdens between the two runs become evident after 2006. In contrast to the burden, the yearly averaged AODs simulated in the two runs are not significantly different, and the yearly trends are similar over China. The burdens of secondary aerosols (sulfate, nitrate, and ammonium) are less sensitive to the emission perturbation than the primary aerosols (BC and POM). This is probably because secondary aerosols experience more complex aerosol processes, such as oxidation of the precursor gases, aerosol nucleation and condensational growth in the gas-phase, and cloud/aqueous-phase chemistry. Nevertheless, significant positive correlations between aerosol burden and emission perturbation are found almost everywhere in China for both primary and secondary aerosols.

This research highlights the simulated AOD biases over China by CESM2. Many AerChemMIP models also suffer from similar biases as CESM2 (not shown here). Difficulties in modeling aerosol properties over China by global climate models have been recognized since CMIP5. Attempts were made to improve aerosol simulation over China in CESM version 1 by introducing a new emission inventory (Fan et al., 2018) and adding nitrate aerosols (Lu et al., 2021). However, our results shows that CESM2, the successor of CESM1, still underestimates AOD over eastern China. We suggest that the bias in the simulated meteorological fields may be more responsible for the AOD bias than emission. This reminds us that, despite improvements in the emission inventory since CMIP5, aerosol modeling biases over China remain. Further investigation of aerosol simulations over China should be applied to other AerChemMIP and CMIP6 models to identify their common issues. The influence of the model biases revealed in this study on aerosol radiative forcing should be evaluated.

Data availability statement

The CMIP6 emission inventory used by CESM2 is downloaded via SVN with the CESM2 release. The gridded emission dataset from the CEDS Project for use in CMIP6 historical and preindustrial control runs is distributed through the Earth System Grid Federation (ESGF). The CESM2 source code and datasets was released to the community in June 2018 (available at www.cesm.ucar.edu:/models/cesm2/). The MEIC and MIC emission inventories are obtained from the MEIC webpage (http://www.meicmodel.org). The global emission dataset that was merged with MEIC for the 30-year period (1986–2015) is available upon request (contact fantianyi@bnu.edu.cn).

Acknowledgements. We greatly appreciate the constructive comments and suggestions from the two reviewers. The authors would like to thank Dr. Zheng LU for providing the CESM2 version that incorporates the MOSAIC module. Special thanks to Dr. Bo ZHENG in the MEIC team for the discussion on details about the scaling process of CEDS to MEIC. This work is supported by the State Key Program of National Natural Science Foundation of China (Grant No. 41830966). Tianyi FAN is supported by the National Natural Science Foundation of China (Grant Nos. 2017YFC1501403, 42030606, and 41705125).

Electronic supplementary material: Supplementary material is available in the online version of this article at https://doi.org/10.1007/s00376-021-1119-6.

REFERENCES

Adler, R. F., and Coauthors, 2018: The Global Precipitation Climatology Project (GPCP) monthly analysis (New Version 2.3) and a review of 2017 global precipitation. *Atmosphere*, **9**, 138, https://doi.org/10.3390/atmos9040138.

Bhartia, P. K., 2002: OMI algorithm theoretical basis document Volume II: OMI ozone products, ATBD-OMI-02, Version 2.0. [Available from https://eospso.gsfc.nasa.gov/sites/default/files/atbd/ATBD-OMI-02.pdf]

Bond, T. C., E. Bhardwaj, R. Dong, R. Jogani, S. Jung, C. Roden, D. G. Streets, and N. M. Trautmann, 2007: Historical emissions of black and organic carbon aerosol from energy-related combustion, 1850–2000: Historical BC/OC emissions. *Global Biogeochemical Cycles*, **21**(2), GB2018, https://doi.org/10.1029/2006GB002840.

Collins, W. J., and Coauthors, 2017: AerChemMIP: Quantifying the effects of chemistry and aerosols in CMIP6. *Geoscientific Model Development*, **10**, 585–607, https://doi.org/10.5194/gmd-10-585-2017.

Danabasoglu, G., and Coauthors, 2020: The community earth system model version 2 (CESM2). *Journal of Advances in Modeling Earth Systems*, **12**, e2019MS001916, https://doi.org/10.1029/2019MS001916.

EC-JRC/PBL, 2012: Emissions Database for Global Atmospheric Research (EDGAR), release EDGARv4.2 FT2012. [Available from http://edgar.jrc.ec.europa.eu]

Emmons, L. K., and Coauthors, 2020: The chemistry mechanism in the community earth system model version 2 (CESM2). *Journal of Advances in Modeling Earth Systems*, **12**, e2019MS001882, https://doi.org/10.1029/2019MS001882.

Eyring, V., S. Bony, G. A. Meehl, C. A. Senior, B. Stevens, R. J. Stouffer, and K. E. Taylor, 2016: Overview of the Coupled Model Intercomparison Project Phase 6 (CMIP6) experimental design and organization. *Geoscientific Model Development*, **9**, 1937–1958, https://doi.org/10.5194/gmd-9-1937-2016.

Fan, T., and Coauthors, 2018: Emission or atmospheric processes? An attempt to attribute the source of large bias of aerosols in eastern China simulated by global climate models.

Atmospheric Chemistry and Physics, **18**, 1395–1417, https://doi.org/10.5194/acp-18-1395-2018.

Feng, L. Y., and Coauthors, 2020: The generation of gridded emissions data for CMIP6. *Geoscientific Model Development*, **13**, 461–482, https://doi.org/10.5194/gmd-13-461-2020.

Forster, P., and Coauthors, 2007: Changes in atmospheric constituents and in radiative forcing. *Climate Change 2007: The Physical Science Basis. Contribution of Working Group I to the Fourth Assessment Report of the IPCC*, S. Solomon et al., Eds., Cambridge University Press, Cambridge, United Kingdom and New York, NY, USA.

Gettelman, A., and H. Morrison, 2015: Advanced two-moment bulk microphysics for global models. Part I: Off-line tests and comparison with other schemes. *J. Climate*, **28**, 1268–1287, https://doi.org/10.1175/JCLI-D-14-00102.1.

Golaz, J.-C., V. E. Larson, and W. R. Cotton, 2002: A PDF-based model for boundary layer clouds. Part I: Method and model description. *J. Atmos. Sci.*, **59**, 3540–3551, https://doi.org/10.1175/1520-0469(2002)059<3540:APBMFB>2.0.CO;2.

Goldewijk, K. K., A. Beusen, G. van Drecht, and M. de Vos, 2011: The HYDE 3.1 spatially explicit database of human-induced global land-use change over the past 12,000 years. *Global Ecology and Biogeography*, **20**, 73–86, https://doi.org/10.1111/J.1466-8238.2010.00587.X.

Hersbach, H., and Coauthors, 2019: ERA5 monthly averaged data on pressure levels from 1979 to present. Copernicus Climate Change Service (C3S) Climate Data Store (CDS), https://doi.org/10.24381/cds.6860a573.

Hoesly, R. M., and Coauthors, 2018: Historical (1750–2014) anthropogenic emissions of reactive gases and aerosols from the Community Emissions Data System (CEDS). *Geoscientific Model Development*, **11**, 369–408, https://doi.org/10.5194/gmd-11-369-2018.

Lamarque, J.-F., and Coauthors, 2013: The Atmospheric Chemistry and Climate Model Intercomparison Project (ACCMIP): Overview and description of models, simulations and climate diagnostics. *Geoscientific Model Development*, **6**, 179–206, https://doi.org/10.5194/gmd-6-179-2013.

Larson, V. E., 2017: CLUBB-SILHS: A parameterization of subgrid variability in the atmosphere. arXiv:1711.03675v2.

Lei, Y., Q. Zhang, K. B. He, and D. G. Streets, 2011: Primary anthropogenic aerosol emission trends for China, 1990-2005. *Atmospheric Chemistry and Physics*, **11**, 931–954, https://doi.org/10.5194/acp-11-931-2011.

Levy, R. C., S. Mattoo, L. A. Munchak, L. A. Remer, A. M. Sayer, F. Patadia, and N. C. Hsu, 2013: The Collection 6 MODIS aerosol products over land and ocean. *Atmospheric Measurement Techniques*, **6**, 2989–3034, https://doi.org/10.5194/amt-6-2989-2013.

Li, J. W., and Z. W. Han, 2012: A modeling study of seasonal variation of atmospheric aerosols over East Asia. *Adv. Atmos. Sci.*, **29**(1), 101–117, https://doi.org/10.1007/s00376-011-0234-1.

Li, M., and Coauthors, 2014: Mapping Asian anthropogenic emissions of non-methane volatile organic compounds to multiple chemical mechanisms. *Atmospheric Chemistry and Physics*, **14**, 5617–5638, https://doi.org/10.5194/acp-14-5617-2014.

Li, M., and Coauthors, 2017: MIX: A mosaic Asian anthropogenic emission inventory under the international collaboration framework of the MICS-Asia and HTAP. *Atmospheric Chemistry and Physics*, **17**, 935–963, https://doi.org/10.5194/acp-17-935-2017.

Liu, F., Q. Zhang, D. Tong, B. Zheng, M. Li, H. Huo, and K. B. He, 2015: High-resolution inventory of technologies, activities, and emissions of coal-fired power plants in China from 1990 to 2010. *Atmospheric Chemistry and Physics*, **15**, 13299–13317, https://doi.org/10.5194/acp-15-13299-2015.

Liu, J. J., Y. F. Zheng, Z. Q. Li, C. Flynn, and M. Cribb, 2012a: Seasonal variations of aerosol optical properties, vertical distribution and associated radiative effects in the Yangtze Delta region of China. *J. Geophys. Res.: Atmos.*, **117**, D00K38, https://doi.org/10.1029/2011JD016490.

Liu, X., P.-L. Ma, H. Wang, S. Tilmes, B. Singh, R. C. Easter, S. J. Ghan, and P. J. Rasch, 2016: Description and evaluation of a new four-mode version of the Modal Aerosol Module (MAM4) within version 5.3 of the Community Atmosphere Model. *Geoscientific Model Development*, **9**, 505–522, https://doi.org/10.5194/gmd-9-505-2016.

Liu, X., and Coauthors, 2012b: Toward a minimal representation of aerosols in climate models: Description and evaluation in the Community Atmosphere Model CAM5. *Geoscientific Model Development*, **5**, 709–739, https://doi.org/10.5194/gmd-5-709-2012.

Lu, Z., X. H. Liu, R. A. Zaveri, R. C. Easter, S. Tilmes, L. K. Emmons, and Coauthors, 2021: Radiative forcing of nitrate aerosols from 1975 to 2010 as simulated by MOSAIC module in CESM2-MAM4. *J. Geophys. Res.: Atmos*, **126**, e2021JD034809, https://doi.org/10.1029/2021JD034809.

Park, S. S., T. Takemura, and S.-W. Kim, 2018: Comparison of aerosol optical depth between observation and simulation from MIROC-SPRINTARS: Effects of temporal inhomogeneous sampling. *Atmos. Environ.*, **186**, 56–73, https://doi.org/10.1016/j.atmosenv.2018.05.021.

Randles, C. A., and Coauthors, 2017: The MERRA-2 aerosol reanalysis, 1980 onward. *Part I: System description and data assimilation evaluation. J. Climate*, **30**, 6823–6850, https://doi.org/10.1175/JCLI-D-16-0609.1.

Remer, L. A., and Coauthors, 2008: Global aerosol climatology fromthe MODIS satellite sensors. *J. Geophys. Res.: Atmos.*, **113**, D14S07, https://doi.org/10.1029/2007JD009661.

Sayer, A. M., L. A. Munchak, N. C. Hsu, R. C. Levy, C. Bettenhausen, and M.-J. Jeong, 2014: MODIS Collection 6 aerosol products: Comparison between Aqua's e-Deep Blue, Dark Target, and "merged" data sets, and usage recommendations. *J. Geophys. Res.: Atmos.*, **119**, 13965–13989, https://doi.org/10.1002/2014JD022453.

Schutgens, N. A. J., D. G. Partridge, and P. Stier, 2016: The importance of temporal collocation for the evaluation of aerosol models with observations. *Atmospheric Chemistry and Physics*, **16**, 1065–1079, https://doi.org/10.5194/acp-16-1065-2016.

Shindell, D. T., and Coauthors, 2013: Radiative forcing in the ACCMIP historical and future climate simulations. *Atmospheric Chemistry and Physics*, **13**, 2939–2974, https://doi.org/10.5194/acp-13-2939-2013.

Smith, C. J., and Coauthors, 2020: Effective radiative forcing and adjustments in CMIP6 models. *Atmospheric Chemistry and Physics*, **20**, 9591–9618, https://doi.org/10.5194/acp-20-9591-2020.

Streets, D. G., Q. Zhang, L. T. Wang, K. B. He, J. M. Hao, Y. Wu, Y. H. Tang, and G. R. Carmichael, 2006: Revisiting China's CO emissions after the Transport and Chemical Evolution over the Pacific (TRACE-P) mission: Synthesis of inventories, atmospheric modeling, and observations. *J. Geophys.*

Res.: Atmos., **111**, D14306, https://doi.org/10.1029/2006JD007118.

van Marle, M. J. E., and Coauthors, 2017: Historic global biomass burning emissions for CMIP6 (BB4CMIP) based on merging satellite observations with proxies and fire models (1750–2015). *Geoscientific Model Development*, **10**, 3329–3357, https://doi.org/10.5194/gmd-10-3329-2017.

Wang, S. W., and Coauthors, 2012: Growth in NO_x emissions from power plants in China: Bottom-up estimates and satellite observations. *Atmospheric Chemistry and Physics*, **12**, 4429–4447, https://doi.org/10.5194/acp-12-4429-2012.

Wu, M. X., and Coauthors, 2020: Understanding processes that control dust spatial distributions with global climate models and satellite observations. *Atmospheric Chemistry and Physics*, **20**, 13835–13855, https://doi.org/10.5194/acp-20-13835-2020.

Yang, Y., L. M. Russell, S. J. Lou, H. Liao, J. P. Guo, Y. Liu, B. Singh, and S. J. Ghan, 2017: Dust-wind interactions can intensify aerosol pollution over eastern China. *Nature Communications*, **8**, 15333, https://doi.org/10.1038/ncomms15333.

Zhang, Q., D. G. Streets, K. B. He, and Z. Klimont, 2007a: Major components of China's anthropogenic primary particulate emissions. *Environmental Research Letters*, **2**, 045027, https://doi.org/10.1088/1748-9326/2/4/045027.

Zhang, Q., and Coauthors, 2007b: NO_x emission trends for China, 1995–2004: The view from the ground and the view from space. *J. Geophys. Res.: Atmos.*, **112**, D22306, https://doi.org/10.1029/2007JD008684.

Zhang, Q., and Coauthors, 2009: Asian emissions in 2006 for the NASA INTEX-B mission. *Atmospheric Chemistry and Physics*, **9**, 5131–5153, https://doi.org/10.5194/acp-9-5131-2009.

Zhang, R., and Coauthors, 2013: Chemical characterization and source apportionment of $PM_{2.5}$ in Beijing: Seasonal perspective. *Atmospheric Chemistry and Physics*, **13**, 7053–7074, https://doi.org/10.5194/acp-13-7053-2013.

Zheng, B., H. Huo, Q. Zhang, Z. L. Yao, X. T. Wang, X. F. Yang, H. Liu, and K. B. He, 2014: High-resolution mapping of vehicle emissions in China in 2008. *Atmospheric Chemistry and Physics*, **14**, 9787–9805, https://doi.org/10.5194/acp-14-9787-2014.

Ziemke, J. R., S. Chandra, G. J. Labow, P. K. Bhartia, L. Froidevaux, and J. C. Witte, 2011: A global climatology of tropospheric and stratospheric ozone derived from Aura OMI and MLS measurements. *Atmospheric Chemistry and Physics*, **11**, 9237–9251, https://doi.org/10.5194/acp-11-9237-2011.